Mechanical transduction via a single soft polymer

Ruizheng Hou,[1,*] Nan Wang,[2] Weizhu Bao,[2,3] and Zhisong Wang[3,4]

[1]*School of Science and Institute of Quantum Optics and Quantum Information, Xi'an Jiaotong University, Shaan Xi 710049, China*
[2]*Department of Mathematics, National University of Singapore, Singapore 119076*
[3]*NUS Graduate School for Integrative Sciences and Engineering, National University of Singapore, Singapore 119076*
[4]*Department of Physics, National University of Singapore, Singapore 117542*

Molecular machines from biology and nanotechnology often depend on soft structures to perform mechanical functions, but the underlying mechanisms and advantages or disadvantages over rigid structures are not fully understood. We report here a rigorous study of mechanical transduction along a single soft polymer based on exact solutions to the realistic three-dimensional wormlike-chain model and augmented with analytical relations derived from simpler polymer models. The results reveal surprisingly that a soft polymer with vanishingly small persistence length below a single chemical bond still transduces biased displacement and mechanical work up to practically significant amounts. This "soft" approach possesses unique advantages over the conventional wisdom of rigidity-based transduction, and potentially leads to a unified mechanism for effective allosterylike transduction and relay of mechanical actions, information, control, and molecules from one position to another in molecular devices and motors. This study also identifies an entropy limit unique to the soft transduction, and thereby suggests a possibility of detecting higher efficiency for kinesin motor and mutants in future experiments.

I. INTRODUCTION

Unlike macroscopic machines and devices made of rigid materials, molecular counterparts from biology and nanotechnology often depend on soft structures to perform mechanical functions. Indeed, soft polymers like peptides, nucleotides, and synthetic polymers execute mechanical actions and transduction in biological molecular motors [1–4] as well as rationally designed nanomotors [5–20] and simpler force-generating or actuating devices [21–23] from DNA nanotechnology and supramolecular chemistry. Soft polymers are also used in nonmotor applications to transmit mechanical actions, control, information, and molecular agents from one location to another. Examples include mechanical transduction via polymer brushes, collectively [24], remote asymmetric control [25,26] through a single flexible molecular linker for the purpose of chemical synthesis, distant intramolecular relay of information [27,28] based on steric hindrance between nearest neighbors, and site-specific delivery of molecules [29] by a swinging polymer immobilized at one end.

Perhaps the most remarkable example for polymer-based transduction is offered by motor protein kinesin, which is a bipedal walker doing intracellular transport along cytoskeletal tracks. Kinesin's two identical legs are connected by two peptide chains called neck linkers that are interwound into a coiled coil bundle in the middle of the walker. During kinesin's walking, a track-bound leg aligns a part of its neck linker in a zipperlike manner along the polar track to position [2] the other leg forward, and transmit an intrachain force against a load. This polymer-based transduction is notable for multiple reasons. First, the neck linkers are very soft, with a persistence length of ∼1 nm versus a total contour length of 10 times as long. Second, the transduction is repeatable as both the neck linker and the track-bound leg remain intact when the latter catalyzes reaction of a chemical fuel driving the zippering. Third, the end-to-end transduction started from an active control (i.e., zippering) may be regarded as a generalized allosteric control through an entirely disordered and open polymer, while the allosteric control [30] by its conventional definition occurs within the close-packed structure of a folded protein molecule.

The zippering effect, if taken out of the specific context of kinesin motor and placed in a wider perspective, can be generalized into a single-way downhill transduction from an actively imposed orientation control at one end of a single soft polymer to mechanical outcomes at the other end (i.e., biased positioning and force). Such an orientation-based intramolecular transduction has the potential to serve as a unified physical mechanism for allosterylike transduction of positioning, force, information and control, and molecular agents beyond steric effects and in a repeatable manner. This is because the transduced biased positioning and force can further generate mechanical work, encode information, and facilitate control or molecular delivery.

For macroscopic machines or devices, it is common wisdom to use rigid components instead of soft ones for effective mechanical transduction. This conventional wisdom holds presumably also for molecular-scale transduction via a single polymer, since thermal fluctuations reshape a soft polymer more easily than a stiff polymer, and hence seriously affect the transduction effectiveness by the former. It remains unclear how to use soft polymers to do effective transduction at the molecular scale, and whether any minimal requirement of the polymer softness exists for practical transduction. It

_____

*houruizheng@xjtu.edu.cn

is even doubtful whether a soft polymer presents any real advantages over a stiff one for polymer-based transduction. These questions touch the fundamental polymer mechanics, and bear far-reaching importance for nanotechnology and biology. These questions are timely as the soft-matter approach [31] to nanotechnology is now becoming widespread, and the recently emerging field of mechanobiology reveals an increasing importance of intrinsically disordered proteins (IDPs [32], which are soft random-coil chains entirely) in mechanics-related functions at the molecular or cellular level.

In this paper, we address the above questions concerning transduction effectiveness of soft polymers through a rigorous study of the generalized orientation-based mechanical transduction. Previous theoretical studies [33–39] on the zippering effect are mostly focused on its role in kinesin's directional rectification, and are done within the context of the motor's chemomechanical cycle. These studies often use polymer models for ideal chains or approximate solution to the more realistic model of wormlike chains (WLCs) [40,41]. We study a general setup for the orientation-based single-way transduction, which may be used within a motor as part of its operation cycle or within simpler devices for relay of positioning, force, information and control, and molecular agents. We obtain the exact solution to the three-dimensional WLC polymer in the transduction setup, which allows a reliable entropy and energy counting necessary for examination of the transduction effectiveness.

In this paper, the exact WLC solution reveals a surprisingly effective transduction even by a soft polymer with a persistence length shorter than a single chemical bond, which virtually covers the softest polymers in practice. This important but counterintuitive finding is validated and conceptually clarified with analytical relations derived from simpler polymer models for freely joined chains [41] and Gaussian chains. These results expose unique advantages of soft polymers versus stiff ones for intramolecular transduction, and have wide implications from biology to nanotechnology.

II. MODEL FOR SINGLE-POLYMER MECHANICAL TRANSDUCTION

Aligning one end of a polymer along a direction may displace the other end forward along the same direction, and produce work by the displacement if an opposing load is present. Hence the orientation control at one end is transduced through the polymer into biased displacement and work production at the other end. The two types of mechanical transduction are studied using a general single-polymer model that mimics the polymer zippering in biomolecular motor kinesin. The model together with kinesin's zippering is illustrated in Fig. 1. In the model, the position and orientation of one end of a polymer are fixed while the other end diffuses freely under thermal fluctuation in an isothermal environment of temperature T. The polymer is modeled as a wormlike chain (WLC) with the fixed end referred to as the A end (at the origin point of the coordinate system and oriented along the z axis) and the free end referred to as the B end. The WLC model is a realistic description of semiflexible polymers using two experimentally accessible parameters: contour length (l_c) quantifying the maximum stretchable length and persistence length (l_p) quantifying the
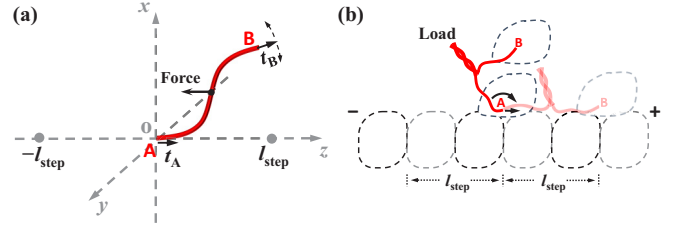

FIG. 1. Illustration of the single-polymer model for orientation-based transduction (a) and the neck linker zippering in kinesin (b). (a) The red line denotes a polymer with one end (A end) fixed at the origin of the coordinate frame (x, y, and z axes) and the other end (B end) free. The two vectors t_A and t_B denote the orientations of the two ends. The force applied in the middle of the polymer represents a mechanical load. The gray spherical symbols on the z axis denote the association units for the B end. (b) The dashed lines indicate the two feet of kinesin and the subunits (α/β tubulin) that compose the track (microtubule filaments). The broad red line is the neck linker which connects the two feet. The black arrow denotes the zippering effect that controls the orientation of the linker. "+" and "−" denote the polarity of the track.

bending rigidity. We extend an exact solution for the two-dimensional (2D) WLC model to the three-dimensional (3D) model and apply it to the specific setup of the model (see Methods). Thus, we are able to rigorously enumerate the bending energy and entropy of the three-dimensional WLC polymer in the setup and with a constant load added to the polymer at any point along its contour. The exact solution yields the position distribution of the B end [$Q(r_B)$] averaged over all possible polymer configurations under a load, thereby allowing evaluation of the displacement or work transduction that is precise within the framework of the WLC model. To assist analysis of the numeric WLC results, the polymer is also modeled using the freely joined-chain (FJC) model that represents completely flexible polymers made of segments of identical length (b) but without any bending rigidity.

We consider the orientation of the A end to be absolutely fixed toward the forward direction of the z axis for the first part of this study (see Results, Secs. III A–III D). This constraint is relaxed later (Sec. III E). For the relevance to small nanomotors and nanodevices, the total contour length (l_c) of the polymer is kept short, which is 10 nm in most of our calculations [except Figs. 4(b) and 4(c)] and all the discussions. The persistence length (l_p) of the WLC and the segment length (b) of the FJC are chosen to be smaller than this contour length (10 nm) for representing soft polymers.

III. RESULTS

A. Transduction of biased displacement

With the A end oriented (t_A) along the z axis, the distribution of the B end [$Q(r_B)$] derived from the 3D WLC model is biased along the z axis [Fig. 2(a)]. The biased displacement is also indicated by the asymmetric profile [$F(z_B) = -k_B T \ln Q(z_B)$] of the polymer free energy versus the position of the B end along the z axis [Fig. 2(b)]. A molecular motor like kinesin often harvests the biased displacement for directional motion by periodic binding sites that capture the polymer's freely diffusing end [Fig. 1(a)]. Now imagine that two binding sites
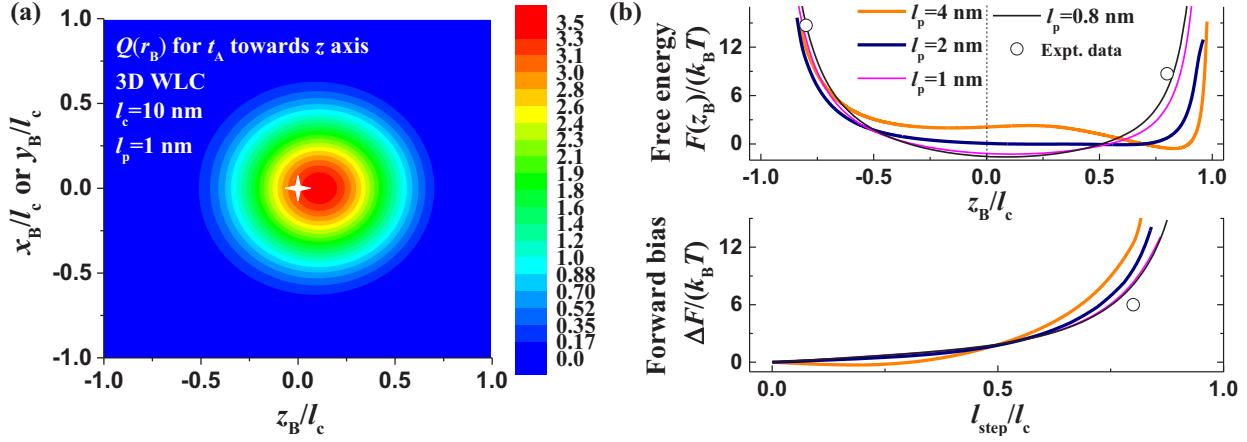
FIG. 2. Biased displacement of the B end. The polymer is modeled as a WLC in 3D space (Fig. 1) with the A end oriented (t_A) along the z axis. The contour length (l_c) of the polymer is 10 nm. (a) The position distribution of the B end in the x-z plane or y-z plane is shown for a persistence length (l_p) of 1 nm. The white cross in the center of the figure marks the origin point of the coordinate system. The overall distribution is symmetric around the z axis. (b) The upper panel shows the free energy of the polymer versus the B-end position along the z axis [$r_B = (0, 0, z_B)$] for different values of persistence length. The symbols are the measured binding barriers [42] for kinesin's mobile foot connected to the other track-bound foot via the neck linker. The lower panel shows the difference between the polymer's free energy when its B end is at a forward site ($z_B = l_{step}$) or an equally distanced backward site ($z_B = -l_{step}$, with l_{step} as the step size).

for the polymer's B end are placed along the z axis before and after the A end by a distance l_{step} [henceforth called step size; see Fig. 1(b)]. The probabilities of the B end moving to the forward site and the backward site are determined by the respective free energies of the polymer. Hence the bias for displacing the free end to the forward site over the backward site is quantified by the free-energy difference at a chosen step size l_{step}, namely, $\Delta F = k_B T [\ln Q(l_{step}) - \ln Q(-l_{step})]$, which is referred to as the bias throughout the paper. The bias increases with the step size, and drops mildly for polymers with shorter persistence length (l_p) [Fig. 2(b)]. After l_p is reduced to 1 nm, a bias of $\sim 8.3 k_B T$ still remains for a modest step size of $l_{step} = 8$ nm for a polymer with a contour length of $l_c = 10$ nm [corresponding to $l_{step}/l_c = 0.8$ in Fig. 2(b)]. This is equivalent to transduction of a forward force of ~ 2.1 pN to the diffusing end of the polymer (at room temperature), as the bias will be compromised if the same amount of opposing force is applied to the same end. While the transduced force appears modest, the transduced bias is rather significant, resulting in a forward versus backward displacement ratio larger than 4000:1. These results indicate that a soft polymer can effectively transduce biased displacement over a large portion of its contour length.

The exact WLC results in Fig. 2 are computed using the same parameters as for kinesin's neck linkers for the sake of comparison with the experimental data on the motor's zippering effect. Kinesin's interleg neck linkers have ~ 28 amino acid residues in total, as reported from previous experiments [2] and are also found compatible with measured leg binding barriers in theoretical studies [35]. The total contour length of kinesin's interleg linkers is $l_c = 28$ amino acids $\times$ 0.36 nm/amino acid ≈ 10 nm (28 amino acids in total and 0.36 nm contour length per amino acid [2,35]). Considering kinesin's measured step size [43] of $l_{step} \approx 8$ nm, the l_{step}/l_c ratio has a value of 0.8. Kinesin's neck linkers have a persistence length [35,44,45] of $l_p \approx 1$ nm, which is rather low compared to the contour length. For the parameters relevant to kinesin's zippering ($l_p = 1$ nm,

$l_{step}/l_c = 0.8$), the bias from the exact WLC results is near the experimentally measured bias ($\sim 6 k_B T$) [42,46,47] [Fig. 2(b), lower panel]. Besides, the asymmetric free-energy profile from the WLC results for the kinesin-relevant parameters predicts a lower barrier for the diffusing end to reach the forward site (at $z_B/l_c = +0.8$) than the backward site (at $z_B/l_c = -0.8$). Both barriers coincide with the measured values [42] [Fig. 2(b)], offering support for reliability of the WLC solution in this study.

Importantly, the experiment-matching bias and barriers are predicted for an orientation control no more than aligning the contour vector associated with the fixed end of the transduction [i.e., t_A in Fig. 1(a) aligned along the z axis]. This amounts to an orientation control within one persistence length, which turns out to be enough for achieving effective transduction up to the level of kinesin's zippering.

The WLC results in Fig. 2(b) indicate that a softer polymer has higher free-energy barriers for large transducing steps with $l_{step} > 0.7 l_c$ ($l_c = 10$ nm). Such barriers are mainly caused by entropy reduction of the polymer during its extension to cover the large transducing steps. Hence, higher barriers indicate fewer probabilities for the polymer to extend, and thereby a longer time for the diffusing end to complete the transduction. For example, a polymer with a very small persistence length of $l_p = 0.25$ nm has a barrier of $\sim 20 k_B T$ to reach the forward site at the transducing step of $0.7 l_c$. For kinesin under an opposing load of ~ 6 pN, the postzippering intramolecular diffusion of the mobile leg encounters the same barrier of $\sim 20 k_B T$, namely, the zero-load barrier [42] of $\sim 8.7 k_B T$ plus the load-induced extra barrier of $\sim 11.7 k_B T$ (i.e., load times kinesin's step size at room temperature). A previous first-passage-time calculation [37] for the mobile leg's intramolecular diffusion found a time of ~ 10 ms to cross the barrier. A simulation study [48] of an artificial protein motor found the same magnitude for the crossing time for a similar barrier. These results suggest that the transduction time for very soft polymers is still fast enough for real applications.
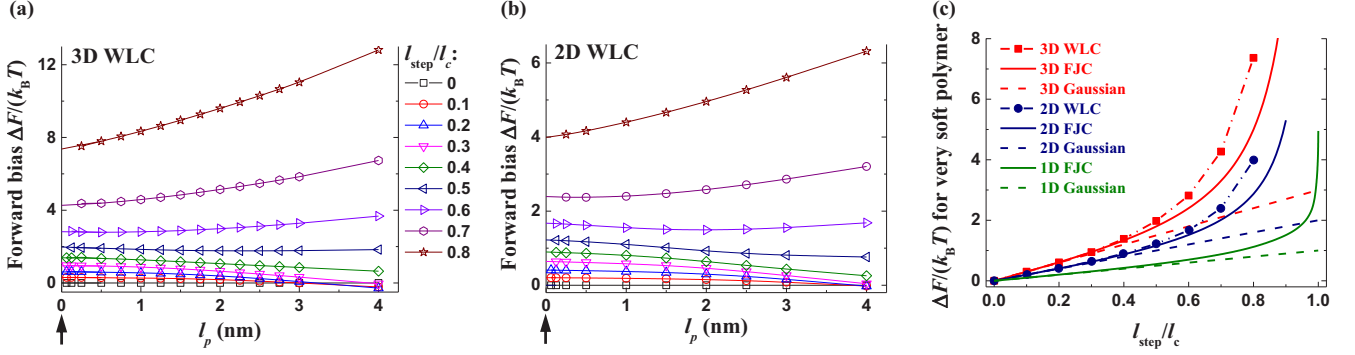
FIG. 3. The bias generated by very soft polymers. The contour length (l_c) of the WLC and the FJC is 10 nm. (a),(b) The bias versus persistence length (l_p) toward the soft-polymer limit ($l_p \to 0$) is shown. The WLC is in 3D space (a) or on a 2D plane (b). The results include biases at nine different step sizes (l_{step}), from $0.8l_c$ to 0 with the interval of $0.1l_c$, which are denoted by different colors and symbols. The symbols are numerical results and the lines are fittings by a fourth-order polynomial function. (c) The symbols are derived by the fittings in (a),(b) at the soft-polymer limit ($l_p \to 0$). The limit is marked by the black arrows in (a),(b). The solid lines are derived from the FJC model at the soft-polymer limit ($b \to 0$). The dashed lines are derived from Gaussian approximation [Eq. (1)] at the same limit.

B. Transduction of biased displacement occurs even for very soft polymers

The persistence length (l_p) is reduced near zero to test whether polymers much softer than biological ones can still transduce the biased displacement. Both the 3D and 2D WLC models predict a nonzero bias with l_p down to 0.1 nm [Figs. 3(a) and 3(b)], which is a hundred times smaller than the polymer's contour length ($l_c = 10$ nm). The persistence length is much smaller than those for biological polymers like peptide and nucleotides. In fact, the l_p value of 0.1 nm is already below the typical length of a single covalent bond [49] (~ 0.15 nm). The bias for such a short persistence length is $\sim 7.3 \, k_B T$ for $l_{step}/l_c = 0.8$. This is a substantial bias, resulting in a forward versus backward displacement ratio of $\sim 1500:1$. Therefore, polymers much softer than biological ones can still transduce biased displacement effectively.

The FJC model also predicts a nonzero bias with the segment length (b) approaching zero [Fig. 3(c), $l_c = 10$ nm]. For comparison to the WLC results, the first FJC segment at the A end, which is set along the z axis, is assigned a half segment length ($b/2$) considering the persistence length–Kuhn length relation ($2l_p = b$) [41]. At short step size, the bias predicted from the FJC model with $b \to 0$ converges with the bias from the WLC model extrapolated at $l_p \to 0$ [Fig. 3(c)]. The convergence at $l_{step} \ll l_c$ is also observed for the bias predicted from Gaussian approximation [41]. Besides, the bias of a three-dimensional WLC polymer is systematically underestimated by the less realistic FJC and Gaussian chain model, and by the reduced models for two-dimensional and one-dimensional polymers [Fig. 3(c)].

While a polymer's free energy includes configurational energy and configurational entropy, the displacement transduction by soft polymers is mainly driven by the entropy change rather than the energy change. The configurational energy of a WLC is proportional to the persistence length (l_p), but the bias (ΔF) is not proportional to the persistence length (l_p) [Figs. 3(a) and 3(b)]. If the configurational energy is instead the major contributor to the bias, reducing l_p from 4 to 1 nm should reduce the bias by three-fourths. But the bias drops to a much lesser extent, and even increases at short step size as shown

by the WLC results [Figs. 3(a) and 3(b)]. Moreover, the finite bias at $l_p \to 0$ is purely contributed by the entropy change. Hence the soft-polymer-based transduction is predominately an entropy effect. This conclusion is supported by the experimentally confirmed [42] entropic nature of zippering-induced bias in kinesin, and is consistent with the successive decrease of predicted biases from three-dimensional polymers to two-dimensional and further one-dimensional polymers [Fig. 3(c)].

C. Analytical relations for displacement bias

To quantify the displacement bias and rationalize the numerical WLC results, we derive analytical relations from the simpler FJC model. In the regime of small displacement ($l_{step} \ll l_c$), Gaussian approximation is valid, yielding the bias (Appendix B 4)

$$\Delta F = 2 n_t n_D k_B T \frac{l_{step}}{l_c - n_t b}. \tag{1}$$

Here b is the Kuhn length ($b = 2l_p$), n_D is the dimension of the polymer ($n_D = 3, 2,$ or 1); n_t is the number of segments oriented along the z axis at the A end of the freely joined chain. Equation (1) shows a finite bias even for extremely soft polymers; i.e., $\Delta F = 2 n_t n_D k_B T l_{step}/l_c$ at $b \to 0$ [shown by dashed lines in Fig. 3(c)].

For large displacement beyond Gaussian approximation, the bias for a one-dimensional FJC follows (Appendix B 3):

$$\Delta F = k_B T \sum_{q=1}^{n_t} \ln \frac{1 + (l_{step} - qb)/(l_c - n_t b)}{1 - (l_{step} + 2b - qb)/(l_c - n_t b)}. \tag{2}$$

For extremely soft polymers ($b \to 0$), Eq. (2) yields a finite bias, too, as $\Delta F = n_t k_B T \ln[(1 + l_{step}/l_c)/(1 - l_{step}/l_c)]$. This relation, which can be expanded as $\Delta F = 2 n_t k_B T (l_{step}/l_c) [1 + \sum_{j=1}^{\infty} (l_{step}/l_c)^{2j}/(2j+1)]$, recovers the result of Gaussian approximation at small l_{step}/l_c. The relation also explains the steep increase of the bias with l_{step}/l_c approaching 1 observed in Fig. 3(c). In Eq. (2), the ratio $(l_{step} - qb)/(l_c - n_t b)$ decreases with increase in b for $l_{step} < l_c$ and $n_t = 1$, resulting in a lower bias for higher b or equivalently higher persistence
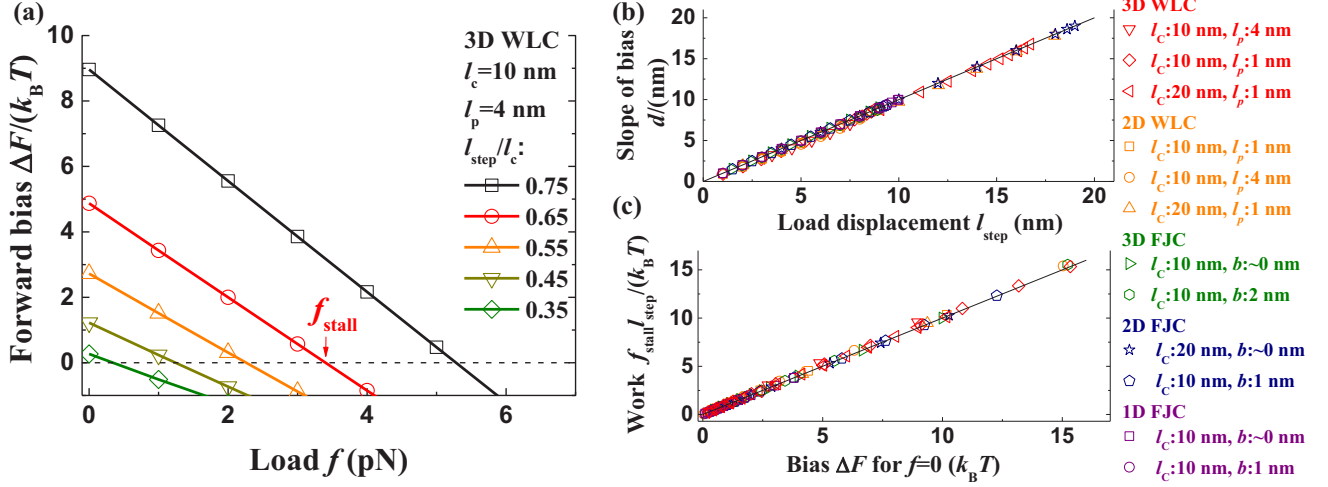
FIG. 4. Transduction of work with load attached in the middle. The contour length of the polymer is 10 or 20 nm as indicated in the figure. (a) Typical load dependences of the bias. The symbols are numerical results from the 3D WLC model and the lines are fittings. (b),(c) Comparison between the decreasing slope (d) of the bias and the load displacement (l_{step}) (b), as well as between the maximum work and the bias without load attached (c). The maximum work is derived by the load (f_{stall}) that cancels the bias (a). The symbols are numerical results and the lines indicate the two quantities in the comparison are equal.

length. This explains the bias decrease against increasing l_p at short step size observed in Figs. 2(b) and 3.

D. Transduction of work

The biased displacement can be harvested to do work if a load is attached to the polymer. Based on a rigorous method for solving WLC [40], we obtain the exact solution for the load-attachment situation. The resulting bias follows a linear dependence on the load [Fig. 4(a)]. Namely, $\Delta F(f) \propto fd$ with the slope (d) depending on the position of load attachment. If the load f is attached to the midpoint of the polymer, the average load displacement is $d_L = l_{step}$ (i.e., half of the B-end displacement) and the work output is $W = fd_L$. If the load is attached at an arbitrary position that is distance s_f from the A end along the polymer contour, the load displacement is $d_L = (2s_f/l_c)l_{step}$. The load displacement matches the slope extracted from the numerically obtained $\Delta F(f)$, namely, $d = d_L$. This holds for load attachment in the middle [Fig. 4(b)], and arbitrary attachment [Fig. 5(a)], for the WLC model and the FJC model, and for a wide range of parameter values (l_{step}, l_c, l_p, or b, including very soft polymers with near-zero l_p or b). If a successive forward step is considered, namely, the A end being free and directed by the now fixed B end to reach the next forward site, the total load displacement is $2l_{step}$ regardless of the location of load attachment (s_f). This load displacement again matches the sum of the two bias slopes.

The numeric results for the bias $\Delta F(f)$ also yield the stall load (f_{stall}) that reduces the bias to zero [i.e., $\Delta F(f_{stall}) = 0$; see Fig. 4(a)]. This stall load determines the maximum work $W_{max} = f_{stall}d_L$. A comparison between the extracted maximum work and the bias without load [$\Delta F(0)$] indicates equality between the two quantities [Figs. 4(c) and 5(b)]. Hence, the work harvested at a finite load equals the bias reduction.

$$W = fd_L = \Delta F(0) - \Delta F(f). \quad (3)$$

The work-bias relation is verified by an analytical formula from the FJC model under Gaussian approximation (Appendix B 4),

$$f\frac{2(s_f - n_t b)}{l_c - n_t b}l_{step} = 2n_t n_D k_B T \frac{l_{step}}{l_c - n_t b} - \Delta F(f). \quad (4)$$

The first term on the left side is the bias without load, $\Delta F(0)$, shown in Eq. (1), and the term on the right side is the work for soft polymers ($b \ll l_c$) and small n_t.
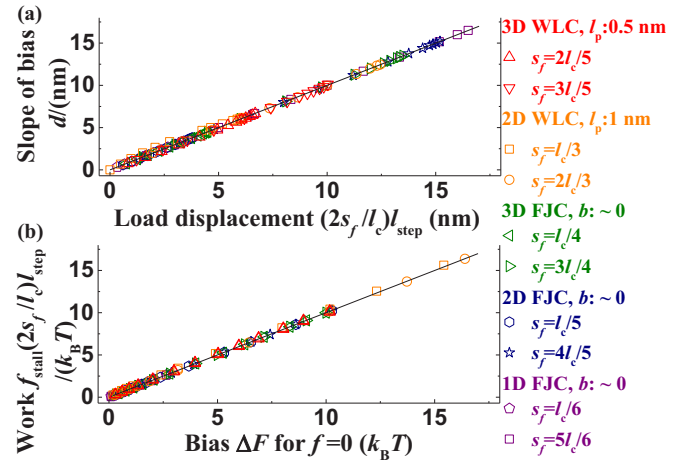

FIG. 5. Transduction of work with load attached arbitrarily. Comparison between the load displacement and the decreasing slope of the bias (a), as well as between the bias without load attached and the maximum work (b). s_f denotes the load-attached location. The colors denote results from different models and with different load-attached locations. The symbols are numerical results and the lines indicate the two quantities in the comparison are equal. The contour length of the polymer is 10 nm.
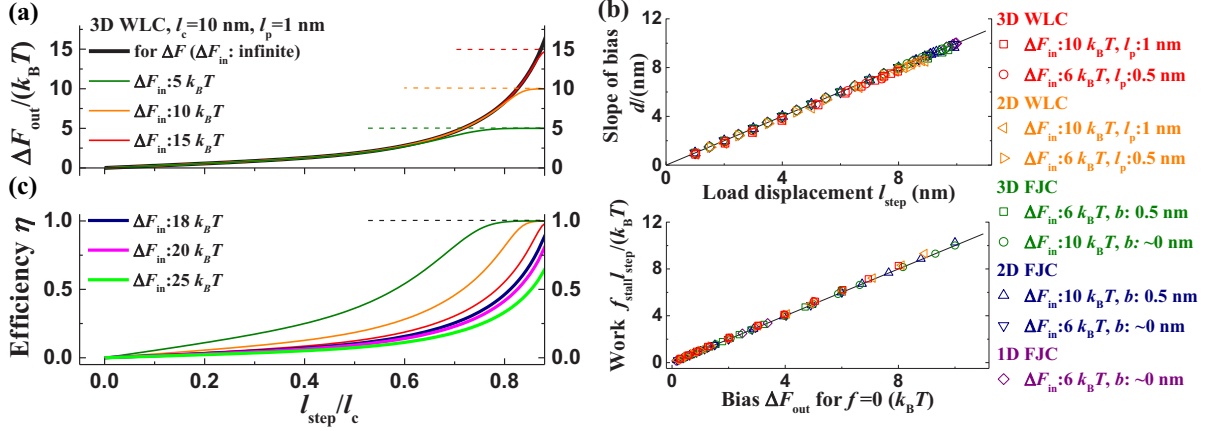
FIG. 6. Limits of work transduction. The contour length of the polymer is 10 nm. (a) Typical results obtained from the 3D WLC model for the displacement bias at the B end (ΔF_{out}) generated from a limited input energy (ΔF_{in}) for controlling the A-end orientation. The maximum displacement bias at the B end (ΔF) generated from the fixed A-end orientation along the z axis (black lines) are shown for comparison. (b) The comparison between the load displacement and the decreasing slope of the bias ΔF_{out} against load (upper panel), as well as between the bias ΔF_{out} with no load attached and the maximum work (lower panel). The load is attached in the middle of the polymer. The symbols are numerical results and the lines indicate equality between the two quantities. (c) Transduction efficiency (η) calculated using Eq. (6) from the results in (a) and similar results for three more ΔF_{in} values.

E. Efficiency of work transduction

The above results show that a soft polymer can transduce an orientation control at one end to mechanical work at another end or an intermediate position along the polymer contour. The previous results are obtained by considering the 100% forward orientation of the polymer's A end along the z axis, which implies an infinitely large energy input to enable the orientation control. In this section, the control at the A end is relaxed to allow both forward and backward orientations along the z axis. Then the energy input for orienting this end forward versus backward is quantified by an orientational bias defined as the free-energy difference $\Delta F_{\text{in}} = k_B T \ln(p_{t\text{A}:z}/p_{t\text{A}:-z})$, where $p_{t\text{A}:z}$ or $p_{t\text{A}:-z}$ is the probability for the A end in the forward or backward orientation ($p_{t\text{A}:z} + p_{t\text{A}:-z} = 1$). The bias ΔF studied in preceding sections is the maximum displacement bias at the B end due to the absolute orientation control under the infinite energy input (i.e., $p_{t\text{A}:z} = 100\%$, $p_{t\text{A}:-z} = 0$, hence infinite ΔF_{in}). When there is a mixed A-end orientation under a finite energy input (i.e., $p_{t\text{A}:z} < 100\%$ and $p_{t\text{A}:-z} > 0$, hence a finite ΔF_{in}), the outcome displacement bias at the B end (ΔF_{out}) depends on the maximum displacement bias (ΔF) and the orientational bias (ΔF_{in}), namely,

$$\Delta F_{\text{out}} = k_B T \ln \frac{e^{(\Delta F_{\text{in}} + \Delta F)/k_B T} + 1}{e^{\Delta F_{\text{in}}/k_B T} + e^{\Delta F/k_B T}}. \quad (5)$$

Equation (5) is general without any dependence on specific polymer models (Appendix C). Equation (5) shows that the outcome bias is not only limited by the input energy ($\Delta F_{\text{out}} < \Delta F_{\text{in}}$), but is also limited by the maximum bias ($\Delta F_{\text{out}} < \Delta F$). Indeed, ΔF_{out} is capped by ΔF_{in} or ΔF, whichever is lower, as shown by the calculations presented in Fig. 6(a). These results help clarify the roles of ΔF_{in} and ΔF in the mechanical transduction: ΔF_{in} is the input which the outcome ΔF_{out}, increasing monotonically with increasing l_{step}/l_c, can approach but never exceed. ΔF is essentially the polymer's inherent maximum

biasing or energy-transducing capacity, which caps the outcome ΔF_{out} even for an infinitely high input ΔF_{in} [Eq. (5)].

When a load is attached to the polymer, the outcome displacement bias at the B end (ΔF_{out}) can convert into work completely. This is because Eq. (3) also holds for ΔF_{out} under a finite energy input, as verified by the calculations presented in Fig. 6(b) (in a way similar to Figs. 4 and 5). Hence the maximum work is $W_{\text{max}} = f_{\text{stall}} d_{\text{L}} = \Delta F_{\text{out}}(f = 0)$. The transduction efficiency, defined as $\eta = W_{\text{max}}/\Delta F_{\text{in}}$, follows as

$$\eta = \Delta F_{\text{out}}(f = 0)/\Delta F_{\text{in}}. \quad (6)$$

As shown by the results in Fig. 6(c), η approaches 100% at a high l_{step}/l_c ratio for $DF_{\text{in}} \leqslant \Delta F$ but remains below 100% for $DF_{\text{in}} > \Delta F$. When the input energy (ΔF_{in}) is within the polymer's transduction capacity (ΔF), all the input energy can be transduced to the work (hence perfect efficiency approachable). However, the efficiency is limited apparently below 100% for an input energy beyond the polymer's transduction capacity (i.e., $DF_{\text{in}} > \Delta F$), as the redundant energy input ($\Delta F_{\text{in}} - \Delta F$) cannot be processed by the polymer and becomes waste. This is because the maximum work is capped by the maximum displacement bias ΔF that a polymer can produce at the B end. Hence a key to promote the transduction efficiency and the total amount of transduced work is to raise ΔF, which is also the polymer's inherent biasing capacity. For a given polymer of a certain bias capacity, the transduction efficiency can be promoted by reducing the energy input as shown by the results in Fig. 6(c). We note that a redundant energy input might be necessary for fast transduction in practice.

IV. DISCUSSIONS

A. Double roles of entropy in mechanical transduction of soft structures

Intuitively, a soft structure is disadvantageous for transducing displacement and work from one end to the other, and

increasingly so when the inner rigidity of the structure becomes vanishingly low. Thus, it is rather a counterintuitive finding that the transduction of biased displacement and work remains effective even for soft polymers with persistence length down to a single chemical bond. The transduced bias and work are both significant in magnitude: The bias is up to 1500:1 for $l_p = 0.15$ nm at $l_{step}/l_c = 0.8$ ($l_c = 10$ nm), and the work ($\sim 7.3 k_B T$) is near two-thirds of the standard free energy change ($\Delta \mu_0$) from ATP hydrolysis, which is a common energy supply for molecular motors in biology ($\Delta \mu_0 \approx 11.2 k_B T$ by averaging the measured values from three different experiments [50–52]). The conclusion of effective transduction by very soft polymers is established from the exact solution for the WLC model and supported by analytical relations derived from the FJC model with and without Gaussian approximation.

The effective transduction prevails even for persistence length or Kuhn length approaching zero, indicating unambiguously an entropy nature of the soft-polymer-based transduction. The precise counting of entropy and energy of a WLC polymer versus its bending rigidity also indicates that the transduced bias and work originate predominantly from the entropy, and hence largely remain when the rigidity becomes vanishingly low. This clarifies the seemingly counterintuitive effectiveness of soft-polymer-based transduction.

While the relatively large entropy of a very soft polymer enables effective mechanical transduction, the entropy limits the amount of work transduced and thereby the transduction efficiency. The input energy may be arbitrarily high for controlling one end of a polymer, but the transduced work at the other end is capped by the polymer's bias-generating capacity that is in turn limited to a finite value by the entropy nature of the soft-polymer-based transduction. As shown in Fig. 6, the transduction efficiency is capped apparently below 100% when the input energy exceeds the finite bias capacity, which is determined by the polymer's intrinsic entropy (i.e., its number of possible configurations under the applied control).

The entropy-enabled transduction of soft polymers is essentially different from the rigidity-based transduction of solid parts in macroscopic machines. The entropy limit for work is lost for rigid structures as they are dominated by enthalpy rather than entropy. The transduction through an infinitely rigid polymer is equivalent to the transduction enabled by aligning a polymer's entire contour length along a direction. Equation (1) yields an infinite bias capacity in this situation (i.e., under the condition $n_t b = l_c$). Hence the limit to work is lost for completely rigid structures, allowing arbitrary amounts of work outcome and up to 100% efficiency.

B. Unified transduction and relay mechanism

The results of this study show that controlling the orientation of a soft polymer at one end can transduce to the other end a nontrivial amount of positioning bias (above 1000:1 forward-to-backward displacement ratio), work (several $k_B T$), and force (a few pN), which are enough to trigger downstream molecular events for other purposes such as propagated control and information encoding. Moreover, the transduction readily completes within milliseconds. Therefore, the orientation-based intramolecular transduction provides a unified mechanism for effective allosterylike transduction and relay of

positioning, work, force, information, control, and molecular agents. This unified mechanism covers a wide range of applications, including transduction of mechanical actions (biased positioning, work, force) in molecular motors or simpler nanoactuators [24], remote point-to-point control [25,26] (e.g., via the polymer-transduced force and positioning), information relay [27,28] or signal transduction, site-specific delivery of molecules [29] (e.g., in nanoassembly lines [53]), sensing (e.g., by site-specifically concentrating target molecules for higher detection sensitivity), and sorting of molecular cargos (e.g., on nanorobotic platforms [54]).

These applications mostly have been demonstrated experimentally using other mechanisms, including steric hindrance [27,28] between closely packaged neighbors, chemical mechanisms [9,18,25,26,55] that inflict permanent changes to prevent repeatable operation, or by random intramolecular diffusion [29], etc. The orientation-based transduction is an alternative mechanism for actively controlled, repeatable, and long-range operation. This mechanism was not unimaginable previously after the discovery of kinesin's zippering effect, but little experimental work has been done due to technical difficulty as well as doubts of practical gain, perhaps. This paper's finding of effective transduction even for an extremely soft polymer removes the doubts, reduces the rigidity requirement, and drastically widens the pool of candidate polymers for experimental implementation. Furthermore, the unified mechanism enables development of modularized single-polymer transducers or relay units, which might serve as a standard machine part for flexible use in many molecular devices or motors.

C. Soft-polymer versus stiff-polymer regimes for molecular transducers or relay units

The technical difficulty to implement the transducers and relay units is further reduced by the discovered usefulness of very soft polymers. Indeed, the soft-polymer regime for intramolecular transduction and relay possesses some advantages over the conventional wisdom of using a stiff polymer for the purpose. A transducer or relay unit with a swing soft polymer requires less space to operate than that with a stiff polymer of the same contour length. Reducing the persistence length for the polymer also reduces the required length for orientation control, which may be within a single persistence length from one end of the polymer as found by this study. Therefore, compared to the stiff-polymer regime, the soft-polymer regime likely reduces implementation requirements and leads to drastically downsized transducers or relay units, which amount to a big advantage for operation within a crowded environment in nanotechnological applications.

Not accidently, perhaps, the smallest motor protein discovered from intracellular transport is kinesin, which uniquely employs a soft interleg chain for orientation-based transduction. Other motor proteins like dyneins [4] and myosins [56,57] use instead a much more rigid interleg connection (e.g., coiled coils [58]). Interestingly, kinesin and the much bigger cytoplasmic dynein walk on the same cytoskeletal track toward the opposite direction, but kinesin produces a higher force [59,60] when both are caught in a tug of war. It is thus desirable to develop artificial nanowalkers mimicking kinesin, but no one has yet been successful to date. As a partial kinesin mimic, one DNA

bipedal walker [13–15] uses a local downhill migration of a track-bound leg to bias the other leg forward along a polar DNA track through a soft interleg linker (nucleotide chain). This and other artificial nanowalkers are still far behind kinesin in performance (e.g., directionality [10,11,17], speed [13,17], and efficiency [17]). Their improvements [61,62] will be helped by this study in some aspects.

In fact, kinesin's individual leg (motor domain) plus the adjacent neck linker (i.e., half of the dimeric kinesin motor) has the potential to be reconstituted into a man-made setup for a small-sized, chemically driven transducer and relay unit for nanotechnological applications. A single-polymer transducer and relay unit also can be engineered from other proteins [63] that are known to bind peptides or single-stranded nucleotides toward a well-defined orientation. Entirely artificial transducers and relay units may be constructed, too, using synthetic molecules and polymers capable of oriented binding, which might be controlled not only by chemical fuels but also by other means like light irradiation [13,19] and pH values [64]. A conceptual framework for these future developments is provided by the entropy limit to the bias capacity. Quantitative guidelines are offered by the relations between this limit and key design parameters (e.g., persistence length and contour length of the transducing polymer and the targeted transduction distance), which are captured by the exact three-dimensional WLC solution or analytically derived from reduced polymer models.

Besides, the soft-polymer versus stiff-polymer regimes might be further studied in future experiments using rigid double-stranded DNA by exploiting the fact that the polymer effects predicted in this study are largely scalable for different persistence length or contour length. Compared to soft single-stranded DNA and peptide chains, the double-stranded DNA is much more rigid (with a persistence length of ∼50 nm) and bulkier (∼2 nm wide), and thereby easier to image [63] using atomic force microscopy (AFM) on a mica surface. Such a DNA explores the soft-polymer regime when its contour length is far beyond the persistence length, and explores the stiff-polymer regime when the contour length is near the persistence length. The high-resolution images of a long double-stranded DNA in different configurations can be used to extract the position and orientation of the two ends of the DNA. For each recorded configuration, a coordinate system can be set and mapped to the transduction model in this paper [Fig. 1(a)], namely, regarding one end of the DNA as the controlled end and placing it at the original point, and regarding this end's orientation as the z axis. Counting the position of the other end in the coordinate system plus a statistical analysis generates the distribution of $Q(r_B)$, which can be used to test many predictions of this study.

D. Entropy limit for polymer-based transduction likely limits the actual energy input in kinesin motor and mutants

In kinesin, the neck linker zippering is not only for transduction but also the major mechanism to couple the chemical energy from the fuel (ATP, that is, adenosine triphosphate) to mechanical stepping: The neck linker zippering at a track-bound leg is triggered by ATP binding [65] at the leg, and further consolidated by the hydrolysis reaction [66]. The later spontaneous dissociation of the reaction products (ADP and Pi,

for adenosine diphosphate and phosphate) recovers the neck linker's unzipped configuration, as suggested by observed zippering-product correlation [66]. Thus the neck linker's zippering and unzippering are coupled almost with the entire chemical cycle for ATP turnover. As a consequence, although the chemical energy from ATP hydrolysis ($\Delta\mu$) is decided not by the motor but by the external concentrations for ATP, ADP, and phosphate (i.e., $\Delta\mu = \Delta\mu_0 + k_B T \ln\{[\text{ATP}]/[\text{ADP}][\text{Pi}]\}$ with $\Delta\mu_0 \approx 11.2 k_B T$ [50–52]), how much of $\Delta\mu$ becomes the actual energy input for the kinesin motor (denoted $\Delta\mu^*$) is likely modulated by its neck linker zippering and unzippering.

Specifically, the neck linker's biasing capacity, which is an inherent property of the polymer, likely limits the maximum energy input from the ATP binding and hydrolysis, which are two energy-releasing processes coupled to the mobile leg's forward binding to the track. The phosphate dissociation from the previously track-bound leg (now the trailing leg) is coupled with the leg's dissociation off track. The neck linker's biasing capacity is ∼8.3 $k_B T$ from the exact WLC results for the relevant parameters [$l_c \approx 10$ nm, $l_p \approx 1$ nm, $l_{\text{step}} \approx 8$ nm, and $l_{\text{step}}/l_c \approx 0.8$, Fig. 6(a)]. This biasing capacity amounts to the maximum energy consumption associated with the forward leg binding. Then the total actual energy input to kinesin can be roughly estimated using a recent finding [67–69] that kinesin has almost equal energy consumption for the forward leg binding and the trailing leg dissociation. Thus the biasing capacity of the neck linkers implies that $\Delta\mu^*$ is ∼16.6 $k_B T$ at best for kinesin. For a comparison, the total energy from ATP hydrolysis is $\Delta\mu \sim 20 k_B T$ under physiological condition [70] (i.e., [ATP] ∼8 mM, [ADP] ∼8 mM, and [Pi] ∼0.4 mM).

The possibility that kinesin's energy input is limited by the neck linker's biasing capacity is supported by two experimental findings. First, as a common observation [43,46,47] from different labs, increasing $\Delta\mu$ by raising ATP concentration does not increase kinesin's maximum work output (i.e., its stall force times the ∼8 nm step size) proportionally. Instead, the stall force saturates [43] around ∼7.5 pN at the high $\Delta\mu$ limit (for ATP concentration from ∼40 to 2000 μM), corresponding to the highest work output ∼15 $k_B T$ (for room temperature). This work value is near the $\Delta\mu^*$ estimated from the biasing capacity of neck linkers. In a contrast, the maximum work by the 100% efficient $F_0 F_1$ rotor [71] follows closely the change of $\Delta\mu$ with no saturation. Second, the WLC results in Fig. 6(a) show that the biasing capacity drops when the l_{step}/l_c ratio becomes lower, e.g., for longer neck linkers. Such a kinesin mutant was constructed in a recent experiment [72] (with 12 more amino acid residues for the interleg linkers, corresponding to $l_c \approx 14.4$ nm and $l_{\text{step}}/l_c \approx 0.56$). This mutant indeed shows a maximum work lower than that of native kinesin [46,47] (by ∼6 $k_B T$ as estimated from the observed ∼3 pN reduction [72] of stall force). On the other hand, the exact WLC results predict that the bias capacity drops from ∼8.3 to ∼2.5 $k_B T$ from the native neck linker to the mutated one, with the ∼5.8 $k_B T$ gap near the observed work reduction. Interestingly, the partial kinesin-mimicking DNA walker [14,15] also displays the same trend of performance reduction with elongated interfoot linkers.

Hence the neck linker's inherent biasing capacity likely limits the energy input to native kinesin, and even more to the mutant as the latter's biasing capacity is far exceeded by

the fuel energy ($\Delta\mu$). Thus, reducing the excessive $\Delta\mu$ below the neck-linker-imposed limit $\Delta\mu^*$ by concentration adjustment does not necessarily reduce the work output, equivalent to detecting a higher efficiency than previous experiments [42,43,46,73]. Kinesin's efficiency is often estimated [73] as the maximum work divided by $\Delta\mu$, while the maximum work is obtained from the measured stall force times the step size. Then the above prediction can be tested by future single-molecule experiments in which the stall force is measured for kinesin and the mutant with concentration control for ATP, ADP, and phosphate (necessary for determining $\Delta\mu$). Similar experiments have been done for the F_0F_1 rotor [71]. For a rough guideline, $\Delta\mu^* \sim 16\,k_BT$ for native kinesin as discussed above, and $\Delta\mu^* \sim 5\,k_BT$ for the kinesin mutant as crudely estimated in the same way. Lowering $\Delta\mu$ toward and below the thresholds likely leads to a disproportional work drop and thereby detection of a higher efficiency than previously observed for kinesin and the mutant. The room for $\Delta\mu$ adjustment is particularly big for the mutant kinesin, implying a higher chance to verify the prediction.

As an encouraging sign, kinesin's capability for higher efficiency is indeed proven by a recent experiment [74] by Schaeffer and co-workers. They found that kinesin rotates unidirectionally while walking at saturating ATP concentration. The rotational work and translational work then add to yield a higher efficiency than previously believed. Combining this experiment with the above proposal might further raise the efficiency (e.g., by keeping the rotation-enabling ATP concentration but adjusting the products for a lower $\Delta\mu$). Moreover, it is interesting to note that performance improvement by $\Delta\mu$ reduction (via lower fuel concentration) has been observed for a chemically driven autonomous artificial nanowalker [17] (for improved directional bias and speed).

We note that kinesin's "zippering" effect is often likened to a power stroke [2]. In a study [75] based on microscopic reversibility, Astumian concluded that "the elastic energy stored by the molecule and released during the conformational change known as the power stroke is irrelevant for determining the directionality, stopping force, and efficiency" of chemically driven molecular motors. This is because these motors do mechanical motion cyclically by consuming chemical fuels and the chemomechanical cycles for fuel molecule consumption and chemical energy utilization obey microscopic reversibility. Other means of energy supply (e.g., light) are not subject to the microscopic reversibility. Hence he also states that "In contrast to the conclusions for chemical driving, a power-stroke is very important for the directionality and efficiency of light-driven molecular machines and for molecular machines driven by external modulation of thermodynamic parameters."

This study does not contradict Ref. [75] as both studies largely deal with different problems. This study addresses the polymer-based transduction that may be driven by any means. Furthermore, the transduction is mostly studied not as a cycle but as a single-way downhill process for applications like signal transduction. According to Ref. [75], there is no question that the transduction also can be used in a cyclically operated molecular machine driven by a wide range of energy supply (light, magnetic driving, electrical driving, pH change, etc.).

The only crossing point between this study and Astumian's is the prediction of detecting higher efficiency in a chemically

powered kinesin motor based on the findings on the polymer-based transduction. However, this prediction is not made by breaking any microscopic reversibility but in a way conforms to Astumian's formulation in Ref. [75] that links a chemical motor's stopping force (hence maximum work output for motors like kinesin due to its fixed step size) to the chemical energy released from the consumed fuel molecule (i.e., $\Delta\mu$). This quantity, which has nothing to do with the motor but is decided completely by the concentrations of the fuel and reaction products, is treated in Ref. [75] as the amount of chemical energy that enters the microscopic-reversibility constraints on the rate ratios of chemomechanical transitions responsible for the motor's motion (Eq. (1) in Ref. [75]). This is true when the chemical cycle of fuel consumption is perfectly coupled with the motor's mechanical cycle (assumed in Ref. [75]). If the chemomechanical coupling is not perfect for a motor, the amount of energy actually channeled into the motor's motion (and hence into its microscopic-reversibility constraints) is lower than $\Delta\mu$. Then this amount of actually used energy (i.e., $\Delta\mu^*$) should replace $\Delta\mu$ in the microscopic-reversibility constraints for this imperfect motor. As a consequence, $\Delta\mu^*$ should also replace $\Delta\mu$ in Astumian's formula determining the motor's stopping force (or maximum work output equivalently). The present study finds that $\Delta\mu^*$ is subject to a new limit from the motor's polymer construction (denoted as $\Delta\mu^*_{\max}$). If this motor-specific limit is apparently lower than $\Delta\mu$ at saturating fuel concentrations (often used for kinesin experiments), a certain amount of chemical energy, $\Delta\mu - \Delta\mu^*_{\max}$, is always wasted by the motor. Tuning down $\Delta\mu$ near $\Delta\mu^*_{\max}$ by lowering the fuel concentration might present a chance to observe the same work output but less energy input, i.e., higher efficiency. Hence the proposed possibility for higher efficiency in kinesin and mutants is derived from an extra limit to a parameter in Astumian's formulas for work output and microscopic reversibility, without anything against these formulas. Besides, the possible higher efficiency is not based on more work from the actual energy input $\Delta\mu^*$ but on the neck linker's biasing capacity as a possible mechanism to limit $\Delta\mu^*$ below $\Delta\mu$.

Reference [75] often leaves workers in the field wondering whether kinesin has any meaningful reason at all to use the zippering effect. In fact, Ref. [75] casts doubt only on the previously narrow perception of this real polymer effect as a so-called power stroke (i.e., "elastic energy stored by the molecule and released during the conformational change" by Astumian's definition in Ref. [75]). The present study starts to shed light on a new facet of this effect, which is relevant to a motor's performance but in a way not related to any delayed release of stored energy but more pertinent to a material's capacity for energy processing. The polymer limit found in this study is similar to the working substance and the cylinder size that limits the actual amount of heat input into a Carnot engine. Specifically, the heat input ΔQ is capped by the equation of state of the working substance and the cylinder size restricting thermal expansion of the working substance, i.e., $\Delta Q = nRT \ln(V_2/V_1)$ for an ideal gas as the working substance, with R as the gas constant, T the temperature, n the gas's molar number, and V_1 and V_2 as the gas's volume before and after the isothermal expansion. An oversupply of heat, e.g., by redundant fuel burning in an internal combustion engine,

does not increase the effective energy input for the engine but causes detrimental effects (e.g., melting the cylinder for even lower efficiency of the engine). The energy oversupply can be reduced for a macroscopic engine by reducing the amount of fuels burned, and reduced similarly for a molecular motor by reducing the fuel concentration. Although a molecular motor consumes one fuel molecule at a time, the energy from a single fuel molecule ($\Delta\mu$) can be redundant when a motor's maximum work is limited below $\Delta\mu$. Identifying the limiting factors is important for the study of real molecular motors, and the polymer limit to $\Delta\mu^*$ from this study is likely one such limiting factor.

V. CONCLUSION AND PERSPECTIVE

We have carried out a rigorous study of mechanical transduction via a single soft polymer based on the exact solution to the WLC model and augmented by analytical relations derived from the simpler FJC model. The results reveal that soft polymers with a persistence length below a single chemical bond are still able to effectively transduce biased displacement and work, but by an entropy-based mechanism distinctly different from the rigidity-based transduction of solid components in macroscopic machines. The inherent entropy of the transducing polymer imposes a limit to the transduction, but this entropy limit is lost when the polymer becomes entirely rigid. These conclusions hold generally for real polymers as their persistence length is virtually all beyond a single chemical bond.

The findings potentially lead to a unified soft-polymer-based mechanism for allosterylike relay and transduction of mechanical actions, control, information, and molecules from one position to another—a basic nanotechnological capability for wide applications ranging from molecular motors, nanoactuators, signal transduction, and sensing, to molecular delivery or sorting on nanoscale assembly lines or robotic platforms. This study exposes the unique advantages of the "soft" relay and transduction over the conventional wisdom of stiff-polymer-based relay and transduction. While a soft polymer for relay and transduction was not unimaginable previously, serious doubts of practical gain have remained. This study removes the doubt and offers timely guidelines for developing soft transducers and relay units. The entropy limit found in this study provides a conceptual framework for these experimental developments, and also suggests a possibility of detecting higher efficiency for kinesin motor and mutants in future experiments.

APPENDIX A: WORMLIKE-CHAIN MODEL WITH LOAD

A wormlike chain is an elastic structure with bending energy of $\frac{1}{4}(n_D - 1)k_BTl_p\int_0^{l_c}[dt(s)/ds]^2ds$. n_D is the number of dimensions of the chain, t is the tangent vector along the chain's contour, and s denotes a position along the contour. Reference [40] provided an exact solution to $Q(r_B)$. Based on the method, we obtain the solution for a chain with a constant load attached at an arbitrary position along the chain's contour.

1. Three-dimensional chain

For a 3D WLC ($n_D = 3$) with load f attached at s_f and pulling opposite the z axis, $Q(r_B)$ is

$$Q(\vec{r}_B) = C\int_{\vec{t}_A}^{\vec{t}_B} D[\vec{t}(s)]e^{-\frac{l_p}{2}\int_0^{l_c}[\frac{d\vec{t}(s)}{ds}]^2 ds - \frac{1}{k_BT}\int_0^{s_f} ft_z(s)ds}\delta^3\left[\vec{r}_B - \int_0^{l_c}\vec{t}(s)ds\right]. \tag{A1}$$

$\int_{t_B}^{t_A} D[t(s)]$ denotes path integration including all polymer configurations, t_z is the portion of the vector t along the z axis, t_A and t_B denote the vector t at the two ends of the polymer, and C is the normalization factor. The case without load attached is obtained by assigning $f = 0$. A Laplace transformation on $Q(r_B)$ generates $\tilde{p}(f_k)$, namely,

$$\tilde{p}(\vec{f}_k) = \int d\vec{r}e^{\vec{f}_k\cdot\vec{r}_B/l_p}Q(\vec{r}_B) = C\int_{\vec{t}_A}^{\vec{t}_B} D[\vec{\tilde{t}}(\tau)]e^{i\int_0^{-i(s_f/l_c)\beta}\{\frac{1}{2}[\frac{d\vec{\tilde{t}}(\tau)}{d\tau}]^2 + \vec{f}_k\cdot\vec{t}(\tau) - f\cdot\tilde{t}_z(\tau)l_p/k_BT\}d\tau + i\int_{-i(s_f/l_c)\beta}^{-i\beta}\{\frac{1}{2}[\frac{d\vec{\tilde{t}}(\tau)}{d\tau}]^2 + \vec{f}_k\cdot\vec{t}(\tau)\}d\tau},$$

$$\tag{A2}$$

where $\tau = -is/l_c$ and $\beta = l_c/l_p$. If $\tilde{p}(f_k)$ is available, $Q(r_B)$ can be derived by the reversed transformation. The mathematical form of Eq. (A2) indicates the path integration can be interpreted as a quantum spin's evolution $t(\tau)$ with the Lagrangian $(dt/d\tau)^2/2 + f_kt - ft_zl_p/k_BT$ in the period of imaginary time from 0 to $-i(s_f/l_c)\beta$ and further with the Lagrangian $(dt/d\tau)^2/2 + f_kt$ in the proceeding period from $-i(s_f/l_c)\beta$ to $-i\beta$. The Hamiltonians corresponding to the Lagrangians are

$$H_1 = -\frac{1}{2}\nabla^2 - f_{k1}\sin\theta\cos\varphi - f_{k2}\sin\theta\sin\varphi - \left(f_{k3} - \frac{fl_p}{k_BT}\right)\cos\theta, \quad [\tau: 0 \text{ to} -i(s_f/l_c)\beta],$$

$$H_2 = -\frac{1}{2}\nabla^2 - f_{k1}\sin\theta\cos\varphi - f_{k2}\sin\theta\sin\varphi - f_{k3}\cos\theta, \quad [\tau: -i(s_f/l_c)\beta \text{ to } -i\beta]. \tag{A3}$$

Hence, $\tilde{p}(f_k)$ is the probability of the spin from the initial orientation t_A evolving to the finial orientation t_B, namely,

$$\tilde{p}(\vec{f}_k) = C\langle \vec{t}_A | e^{-(s_f/l_c)\beta H_1} e^{-(1-s_f/l_c)\beta H_2} | \vec{t}_B \rangle. \tag{A4}$$

$\tilde{p}(f_k)$ is derived using the standard spherical harmonic $Y_l^m(\theta, \varphi)$ as the expansion basis,

$$\tilde{p}(\vec{f}_k) = C \sum_{l,l',l''=0}^{\infty} \sum_{m,m',m''=-l}^{l} \langle \vec{t}_A | Y_{l''}^{m''} \rangle \langle Y_{l''}^{m''} | e^{-(s_f/l_c)\beta H_1} | Y_{l'}^{m'} \rangle \langle Y_{l'}^{m'} | e^{-(1-s_f/l_c)\beta H_2} | Y_l^m \rangle \langle Y_l^m | \vec{t}_B \rangle. \tag{A5}$$

with $\tilde{p}(f_k)$, $Q(r_B)$ derived by the reversed transformation,

$$Q(\vec{r}_B) = \frac{1}{(2\pi l_c)^3} \int \tilde{p}(-iu/\beta) e^{i\vec{u}\cdot\vec{r}_B/l_c} d\vec{u}, \quad (\vec{u} = i\vec{f}_k\beta). \tag{A6}$$

2. Two-dimensional chain

Similar to the 3D case, derivation of $Q(r_B)$ for the 2D WLC still follows the steps above but with all the vectors in 2D and $n_D = 2$. The Hamiltonians for the 2D case are

$$H_1 = -\frac{\partial^2}{\partial\theta} - f_{k1}\sin\theta - \left(f_{k2} - \frac{fl_p}{k_B T}\right)\cos\theta, \quad [\tau: 0 \text{ to} -i(s_f/l_c)\beta],$$

$$H_2 = -\frac{\partial^2}{\partial\theta} - f_{k1}\sin\theta - f_{k2}\cos\theta, \quad [\tau: -i(s_f/l_c)\beta \text{ to} -i\beta]. \tag{A7}$$

$\tilde{p}(f_k)$ for the 2D case is computed using $\varphi_m = 1/\sqrt{2\pi}\, e^{-im\theta}$ for the expansion basis,

$$\tilde{p}(\vec{f}_k) = C \sum_{m,m',m''=-\infty}^{\infty} \langle \vec{t}_A | \varphi_{m''} \rangle \langle \varphi_{m''} | e^{-(s_f/l_c)\beta H_1} | \varphi_{m'} \rangle \langle \varphi_{m'} | e^{-(1-s_f/l_c)\beta H_2} | \varphi_m \rangle \langle \varphi_m | \vec{t}_B \rangle. \tag{A8}$$

$Q(r_B)$ is derived by the reversed transformation similar to Eq. (A6) but for 2D.

3. Computation of $Q(r_B)$

In practical computations, we choose large enough truncation numbers for l and m to ensure the error in Eqs. (A5) and (A8) is negligible. The matrix exponentials $e^{-(sf/lc)\beta H1}$ and $e^{-(1-sf/lc)\beta H2}$ are computed via the Padé approximation. $Q(r_B)$ is obtained from $\tilde{p}(f_k)$ by an inverse fast Fourier transformation.

APPENDIX B: FREELY JOINED-CHAIN MODEL WITH LOAD

A freely joined chain is connected by rigid segments of identical length (b). As the name suggests, bending of the chain does not induce any mechanical force in the connection, so the mechanics of the chain is purely determined by configurational entropy. We apply the method from Ref. [41] to solve the free energy of the chain with load attached.

1. Three-dimensional chain

For deriving the dependence of the free energy on r_B, an extra force (f_k) is attached on the B end, and later the influence of the extra force is removed by a physical relation.

The partition function of the chain with the B end placed on the z axis is

$$Z = \int e^{f_k b/k_B T \sum_{i=1}^{N} \cos\theta_i - f b/k_B T \sum_{i=1}^{N_1} \cos\theta_i} \prod_{i=1}^{N} \sin\theta_i d\theta_i d\varphi_i. \tag{B1}$$

N is the number of segments in the chain and N_1 is the segment where the load (f) is attached. The direction of the load as well as the extra force (f_k) is along the z axis. The free energy with the influence of the extra force is derived by the

partition function,

$$\begin{aligned} G = -k_B T \ln Z = &-N_1 k_B T \ln \frac{4\pi \sinh[(f_k - f)b/k_B T]}{(f_k - f)b/k_B T} \\ &- N_2 k_B T \ln \frac{4\pi \sinh(f_k b/k_B T)}{f_k b/k_B T}, \end{aligned} \tag{B2}$$

where $N_1 + N_2 = N$. r_B is expressed through the free energy and f_k,

$$\begin{aligned} r_B = -\frac{\partial G}{\partial f_k} = &N_1 b\left[\coth\frac{(f_k - f)b}{k_B T} - \frac{k_B T}{(f_k - f)b}\right] \\ &+ N_2 b\left[\coth\frac{f_k b}{k_B T} - \frac{k_B T}{f_k b}\right]. \end{aligned} \tag{B3}$$

The influence of the extra force on the free energy is removed by the relation of $F = G + f_k r_B$.

Equations (B2) and (B3) show F implicitly depends on r_B through f_k. The dependence of $F(r_B, f)$ is obtained numerically. Fixing the orientation of the first n_t segments toward the z axis is equivalent to shifting the profile $F(r_B, f)$ along the direction with a distance of $n_t b$. Meanwhile the contour length is added to by n_t segments, namely, $l_c = (N + n_t)b$. Therefore, the bias generated at step size l_{step} is $\Delta F = F(l_{step} + n_t b, -f) - F(l_{step} - n_t b, f)$.

2. Two-dimensional chain

The partition function for the 2D chain is

$$Z = \int e^{f_k b/k_B T \sum_{i=1}^{N} \cos\theta_i - fb/k_B T \sum_{i=1}^{N_1} \cos\theta_i} \prod_{i=1}^{N} d\theta_i. \quad \text{(B4)}$$

Based on the partition function, the free energy with the influence of the extra force (f_k) is

$$G = -N_1 k_B T \ln \int_0^\pi e^{(f_k - f)b \cos\theta/k_B T} d\theta$$
$$- N_2 k_B T \ln \int_0^\pi e^{f_k b \cos\theta/k_B T} d\theta, \quad \text{(B5)}$$

and the corresponding r_B is

$$r_B = N_1 b \frac{\int_0^\pi e^{(f_k - f)b \cos\theta/k_B T} \cos\theta \, d\theta}{\int_0^\pi e^{(f_k - f)b \cos\theta/k_B T} d\theta}$$
$$+ N_2 b \frac{\int_0^\pi e^{f_k b \cos\theta/k_B T} \cos\theta \, d\theta}{\int_0^\pi e^{f_k b \cos\theta/k_B T} d\theta}. \quad \text{(B6)}$$

With the two equations, the bias ΔF is derived following the procedures for the 3D chain.

3. One-dimensional chain

The 1D FJC model is also called the 1D random-walk model. The free energy and r_B for the 1D chain are

$$G = -N_1 k_B T \ln(e^{(f_k - f)b/k_B T} + e^{-(f_k - f)b/k_B T})$$
$$- N_2 k_B T \ln(e^{f_k b/k_B T} + e^{-f_k b/k_B T}), \quad \text{(B7)}$$

$$r_B = N_1 b \tanh[(f_k - f)b/k_B T]$$
$$+ N_2 b \tanh[f_k b/k_B T]. \quad \text{(B8)}$$

The two equations yield the bias by the same procedures as for the 3D chain.

The load-free bias in Eq. (2) is obtained from the r_B distribution, namely, $Q(r_B) = C \exp\{-\sum_{s=1}^{r_B/2b} \ln[(N+2s)/(N + 2 - 2s)]\}$ with C as the normalization factor. Shifting the profile of $Q(r_B)$ as for the 3D chain yields the bias $\Delta F = k_B T \ln[Q(l_{step} - n_t b)/\ln Q(l_{step} + n_t b)]$, which further leads to Eq. (2).

4. Gaussian approximation to freely joined chains

Under Gaussian approximation, the distribution of r_B without load attached is $Q(r_B) = C \exp[-n_D(r_B/b)^2/(2l_c/b)]$. The bias without load attached is derived by $\Delta F = k_B T \ln Q(l_{step} - n_t b) - k_B T \ln Q(l_{step} + n_t b)$, which leads to Eq. (1).

With load attached, the bias is derived using the partition functions. Take the 3D FJC, for example; under Gaussian approximation ($fd \ll k_B T$ and $f_k d \ll k_B T$) the free energy and r_B for a 3D chain with the extra force (f_k) attached are

$$G = -k_B T \ln 4\pi - \frac{1}{6} N_1 k_B T \left[\frac{(f_k - f)b}{k_B T}\right]^2$$
$$- \frac{1}{6} N_2 k_B T \left(\frac{f_k b}{k_B T}\right)^2, \quad \text{(B9)}$$

$$r_B = Nb \frac{f_k b}{3k_B T} + N_1 b \frac{fb}{3k_B T}. \quad \text{(B10)}$$

Replacing f_k in Eq. (B9) by its form in Eq. (B10) gives the dependence of $G(r_B, f)$, namely,

$$G = -Nk_B T \ln 4\pi - \frac{1}{6} k_B T \left[\frac{9r_B^2}{Nb^2} + \frac{N_1 N_2}{N}\left(\frac{fb}{k_B T}\right)^2\right]. \quad \text{(B11)}$$

The influence of the extra load is removed by $F = G + f_k r_B$, which generates $F(r_B, f)$, namely,

$$F = -k_B T N \ln 4\pi + \frac{3}{2} k_B T \frac{r_B^2}{Nb^2}$$
$$+ \frac{1}{6} k_B T \frac{N_1 N_2}{N}\left(\frac{fb}{k_B T}\right)^2 - \frac{N_1}{N} f r_B. \quad \text{(B12)}$$

Finally the bias is derived by shifting the profile of $F(r_B, f)$, namely, $\Delta F = F(l_{step} + n_t b, -f) - F(l_{step} - n_t b, f)$, which generates Eq. (4) for $n_D = 3$. The bias for the two- and one-dimensional cases ($n_D = 2, 1$) is derived through the above procedures using Eqs. (B5)–(B8).

APPENDIX C: ΔF_{out}-ΔF_{in} RELATION

The general form of the forward versus backward bias for the B end is $\Delta F_{out} = k_B T \ln(p^+/p^-)$, where p^+ and p^- are the respective probabilities of the B end at the forward and backward sites. With the biased orientation of the A end, the probabilities can be expressed by $p^+ = p_{tA:z} p_{tA:z}^+ + p_{tA:-z} p_{tA:-z}^+$ and $p^- = p_{tA:z} p_{tA:z}^- + p_{tA:-z} p_{tA:-z}^-$, where $p_{tA:z}$ and $p_{tA:-z}$ are the probabilities of the A-end orientation toward and opposite the z axis [$\Delta F_{in} = k_B T \ln(p_{tA:z}/p_{tA:-z})$], $p_{tA:z}^+$ and $p_{tA:z}^-$ are the probabilities of the B end at the forward and backward sites when the A-end orientation is toward *the z* axis [$\Delta F = k_B T \ln(p_{tA:z}^+/p_{tA:z}^-)$], and $p_{tA:-z}^+$ and $p_{tA:-z}^-$ are the probabilities of the B end at the forward and the backward sites when the A-end orientation is opposite the z axis. Actually, $p_{tA:-z}^+ = p_{tA:z}^-$ and $p_{tA:-z}^- = p_{tA:z}^+$. Replacing p^+ and p^- by these relations generates Eq. (5).

[1] N. V. DelRosso and N. D. Derr, Curr Opin. Biotechnol. **46**, 20 (2017).

[2] R. D. Vale and R. A. Milligan, Science **288**, 88 (2000).

[3] T. J. Purcell, C. A. Morris, J. A. Spudich, and H. L. Sweeney, Proc. Natl. Acad. Sci. USA **99**, 14159 (2002).

[4] I. R. Gibbons, J. E. Garbarino, C. E. Tan, S. L. Reck-Peterson, R. D. Vale, and A. P. Carter, J Biol. Chem. **280**, 23960 (2005).

[5] W. B. Sherman and N. C. Seeman, Nano Lett. **4**, 1203 (2004).

[6] T. Omabegho, R. Sha, and N. C. Seeman, Science **324**, 67 (2009).

[7] J. S. Shin and N. A. Pierce, J. Am. Chem. Soc. **126**, 10834 (2004).

[8] P. Yin, H. M. T. Choi, C. R. Calvert, and N. A. Pierce, Nature **451**, 318 (2008).

[9] J. Bath, S. J. Green, and A. J. Turberfield, Angew. Chem., Int. Ed. **44**, 4358 (2005).

[10] J. Bath, S. J. Green, K. E. Allen, and A. J. Turberfield, Small **5**, 1513 (2009).

[11] S. J. Green, J. Bath, and A. J. Turberfield, Phys. Rev. Lett. **101**, 238101 (2008).

[12] M. von Delius, E. M. Geertsema, and D. A. Leigh, Nat. Chem. **2**, 96 (2010).

[13] J. Cheng, S. Sreelatha, R. Z. Hou, A. Efremov, R. C. Liu, J. R. van der Maarel, and Z. S. Wang, Phys. Rev. Lett. **109**, 238104 (2012).

[14] M. H. Liu, R. Z. Hou, J. Cheng, I. Y. Loh, S. Sreelatha, J. N. Tey, J. Wei, and Z. S. Wang, ACS Nano **8**, 1792 (2014).

[15] J. Cheng, S. Sreelatha, I. Y. Loh, M. Liu, and Z. S. Wang, Methods **67**, 227 (2014).

[16] I. Y. Loh, J. Cheng, S. R. Tee, A. Efremov, and Z. S. Wang, ACS Nano **8**, 10293 (2014).

[17] M. H. Liu, J. Cheng, S. R. Tee, S. Sreelatha, I. Y. Loh, and Z. S. Wang, ACS Nano **10**, 5882 (2016).

[18] Y. Tian, Y. He, Y. Chen, P. Yin, and C. Mao, Angew. Chem., Int. Ed. **44**, 4355 (2005).

[19] M. You, Y. Chen, X. Zhang, H. Liu, R. Wang, K. Wang, K. R. Williams, and W. Tan, Angew. Chem., Int. Ed. **51**, 2457 (2012).

[20] Q. Y. Yeo, I. Y. Loh, S. R. Tee, Y. H. Chiang, J. Cheng, M. H. Liu, and Z. S. Wang, Nanoscale **9**, 12142 (2017).

[21] J. D. Badjic, V. Balzani, A. Credi, S. Silvi, and J. F. Stoddart, Science **303**, 1845 (2004).

[22] Y. Liu, A. H. Flood, P. A. Bonvallet, S. A. Vignon, B. H. Northrop, H. R. Tseng, J. O. Jeppesen, T. J. Huang, B. Brough, M. Baller, S. Magonov, S. D. Solares, W. A. Goddard, C. M. Ho, and J. F. Stoddart, J. Am. Chem. Soc. **127**, 9745 (2005).

[23] E. R. Kay, D. Leigh, and F. Zerbetto, Angew. Chem., Int. Ed. **46**, 72 (2007).

[24] J. E. Comrie and W. T. S. Huck, Macromol Rapid Commun, **29**, 539 (2008).

[25] P. Linnane, N. Magnus, and P. Magnus, Nature **385**, 799 (1997).

[26] T. Kawasaki, Y. Ishikawa, Y. Minato, T. Otsuka, S. Yonekubo, I. Sato, T. Shibata, A. Matsumoto, and K. Soai, Chem. Eur. J. **23**, 282 (2017).

[27] J. Clayden, A. Lund, L. Vallverdu, and M. Helliwell, Nature **431**, 966 (2004).

[28] L. Byrne, J. Sola, T. Boddaert, T. Marcelli, R. W. Adams, G. A. Morris, and J. Clayden, Angew. Chem., Int. Ed. **53**, 151 (2014).

[29] E. Kopperger, T. Pirzer, and F. C. Simmel, Nano Lett. **15**, 2693 (2015).

[30] J.-P. Changeux and S. J. Edelstein, Science **308**, 1424 (2005).

[31] R. A. L. Jones, *Soft Machines: Nanotechnology and Life* (Oxford University Press, New York, 2004).

[32] H. Jane Dyson and P. E. Wright, Nat. Rev. Mol. Cell Biol. **6**, 197 (2005).

[33] R. F. Fox and M. H. Choi, Phys. Rev. E **63**, 051901 (2001).

[34] W. H. Mather and R. F. Fox, Biophys. J. **91**, 2416 (2006).

[35] Z. S. Wang, M. Feng, W. W. Zheng, and D. G. Fan, Biophys. J. **93**, 3363 (2007).

[36] Z. S. Wang, Proc. Natl. Acad. Sci. USA **104**, 17921 (2007).

[37] D. G. Fan, W. W. Zheng, R. Hou, F. Li, and Z. S. Wang, Biochemistry **47**, 4733 (2008).

[38] W. W. Zheng, D. Fan, M. Feng, and Z. S. Wang, Phys. Biol. **6**, 036002 (2009).

[39] A. Efremov and Z. S. Wang, Phys. Chem. Chem. Phys. **13**, 5159 (2011).

[40] J. Samuel and S. Sinha, Phys. Rev. E **66**, 050801 (2002).

[41] M. Rubinstein, and R. H. Colby, *Polymer Physics* (Oxford University Press, Oxford, 2003).

[42] Y. Taniguchi, M. Nishiyama, Y. Ishii, and T. Yanagida, Nat. Chem. Biol. **1**, 342 (2005).

[43] K. Visscher, M. J. Schnitzer, and S. M. Block, Nature **400**, 184 (1999).

[44] M. S. Z. Kellermayer, S. B. Smith, H. L. Granzier, and C. Bustamante, Science **276**, 1112 (1997).

[45] M. Rief, M. Gautel, F. Oesterhelt, J. M. Fernandez, and H. E. Gaub, Science **276**, 1109 (1997).

[46] N. J. Carter and R. A. Cross, Nature **435**, 308 (2005).

[47] M. Nishiyama, H. Higuchi, and T. Yanagida, Nat. Cell Biol. **4**, 790 (2002).

[48] N. J. Kuwada, M. J. Zuckermann, E. H. C. Bromley, R. B. Sessions, P. M. G. Curmi, N. R. Forde, D. N. Woolfson, and H. Linke, Phys. Rev. E **84**, 031922 (2011).

[49] B. Alberts, A. Johnson, J. Lewis, M. Raff, K. Roberts, and P. Walter, *Molecular Biology of the Cell* (Garland Science, New York, 2002).

[50] J. Rosing and E. Slater, Biochim. Biophys. Acta **267**, 275 (1972).

[51] R. Guynn and R. Veech, J. Biol. Chem. **248**, 6966 (1973).

[52] O. Pänke and B. Rumberg, Biochim. Biophys. Acta **1322**, 183 (1997).

[53] H. Gu, J. Chao, S. J. Xiao, and N. C. Seeman, Nature **465**, 202 (2010).

[54] A. J. Thubagere, W. Li, R. F. Johnson, Z Chen, S. Doroudi, Y. L. Lee, G. Izatt, S. Wittman, N. Srinivas, D. Woods, E. Winfree, and L. Qian, Science **357**, eaan6558 (2017).

[55] K. Lund, A. J. Manzo, N. Dabby, N. Michelotti, A. Johnson-Buck, J. Nangreave, S. Taylor, P. Pei, M. N. Stojanovic, N. G. Walter, E. Winfree, and H. Yan, Nature **465**, 206 (2010).

[56] G. H. Lan and S. X. Sun, Biophys. J. **88**, 999 (2005).

[57] Y. Xu and Z. S. Wang, J. Chem. Phys. **131**, 245104 (2009).

[58] I. Schwaiger, C. Sattler, D. R. Hostetter, and M. Rief, Nat. Mater. **1**, 232 (2002).

[59] C. Kural, H. Kim, S. Syed, G. Goshima, V. I. Gelfand, and P. R. Selvin, Science **308**, 1469 (2005).

[60] V. Belyy, M. A. Schlager, H. Foster, A. E. Reimer, A. P. Carter, and A. Yildiz, Nat. Cell Biol. **18**, 1018 (2016).

[61] T. E. Ouldridge, R. L. Hoare, A. A. Louis, J. P. K. Doye, J. Bath, and A. J. Turberfield, ACS Nano **7**, 2479 (2013).

[62] R. Z. Hou, I. Y. Loh, H. Li, and Z. S. Wang, Phys. Rev. Appl. **7**, 024020 (2017).

[63] A. K. Efremov, Y. Qu, H. Maruyama, C. J. Lim, K. Takeyasu, and J. Yan, J. Biol. Chem. **290**, 15770 (2015).

[64] Y. F. Wang, X. M. Li, X. Q. Liu, and T. H. Li, Chem. Commun. **2007**, 4369.

[65] S. Rice, A. W. Lin, D. Safer, C. L. Hart, N. Naber, B. O. Carragher, S. M. Cain, E. Pechatnikova, E. M. Wilson-Kubalek, M. Whittaker, E. Pate, R. Cooke, E. W. Taylor, R. A. Milligan, and R. D. Vale, Nature **402**, 778 (1999).

[66] B. Milica, J. O. L. Andreasson, W. O. Hancockc, and S. M. Block, Proc. Natl. Acad. Sci. USA **111**, 14136 (2014).

[67] A. Efremov and Z. S. Wang, Phys. Chem. Chem. Phys. **13**, 6223 (2011).

[68] Z. S. Wang, R. Z. Hou, and A. Efremov, J. Chem. Phys. **139**, 035105 (2013).

[69] Z. S. Wang, Integr. Biol. **10**, 34 (2018).

[70] J. Howard, *Mechanics of Motor Proteins and the Cytoskeleton* (Sinauer Associates, Inc., Sunderland, MA, 2001).

[71] S. Toyabe, T. M. Watanabe, T. Okamoto, S. Kudo, and E. Muneyuki, Proc. Natl. Acad. Sci. USA **108**, 17951 (2011).

[72] B. E. Clancy, W. M. Behnke-Parks, J. O. L. Andreasson, S. S. Rosenfeld, and S. M. Block, Nat. Struct. Mol. Biol. **18**, 1020 (2011).

[73] S. M. Block, Trends Cell Biol. **5**, 169 (1995).

[74] A. Ramaiyaa, B. Roya, M. Bugiela, and E. Schaeffer, Proc. Natl. Acad. Sci. USA **114**, 10894 (2017).

[75] R. D. Astumian, Biophys. J. **108**, 291 (2015).